THE UNIVERSITY *of* EDINBURGH

Edinburgh Research Explorer

Wigner-Mott insulator-to-insulator transition at pressure in charge-ordered Fe2OBO3

OPEN ACCESS

Wigner-Mott insulator-to-insulator transition at pressure in charge-ordered Fe$_2$OBO$_3$

G. Diguet,[1] G. R. Hearne,[1,*] W. N. Sibanda,[1] E. Carleschi,[1] P. Musyimi,[1] V. Pischedda,[2] and J. P. Attfield[3]

[1]*Department of Physics, University of Johannesburg, PO Box 524, Auckland Park, 2006, Johannesburg, South Africa*

[2]*Institut Lumière Matière, UMR5306 Université Lyon 1-CNRS, Université de Lyon 69622 Villeurbanne, Cedex, France*

[3]*Centre for Science at Extreme Conditions and School of Chemistry, University of Edinburgh, Erskine Williamson Building, King's Buildings, Mayfield Road, Edinburgh EH9 3JZ, United Kingdom*

Magnetic-electronic studies of mixed-valence Fe$_2$OBO$_3$ have shown that ionic charge order (CO) is disrupted at ~16 GPa. The pertinent minority-spin carrier exhibits persistent intersite electron exchange Fe^{2+} ⇔ Fe^{3+} to well beyond this pressure. Temperature-dependent electrical transport measurements over an extended pressure range presented here demonstrate that the electronic structure remains gapped to well beyond 16 GPa. Extrapolation of data to higher pressure suggests that metallization will only prevail at $P > 50$ GPa. Both the persistent gapped electronic state across the CO instability and signature of carrier confinement to Fe-Fe dimers in the Fe^{2+} ⇔ Fe^{3+} electron exchange are rationalized as crossover from a Wigner crystal (site centered) insulator to a dimer Mott (bond centered type) insulator—"Wigner-Mott transition" at ~16 GPa. The dimer insulating state is a consequence of modulation of the relevant hopping parameter t in quasi-low-dimensional features in the structure (ribbons and chains). Complementary structural studies suggest that the a axis is appreciably more compressible than other crystallographic directions of the original monoclinic unit cell. Therefore, such a modulation in t may arise from Peierls type distortions along the a axis or else stems from intrinsic modulation in the c axis direction of the unit cell. This is aided by a monoclinic ($P2_1/c$) → orthorhombic ($Pmcn$) structural adjustment that is concurrent across the electronic transition. Pressure tuning of relative values of on-site U/t and intersite V/t Coulomb interaction parameters of the quasi-low-dimensional features evolve the system from site-centered to dimer-centered electron localization.

PACS number(s): 84.37.+q, 71.28.+d, 62.50.−p

I. INTRODUCTION

Charge order (CO) states may occur in strongly correlated electron systems to minimize the repulsive energy between valence electrons at the expense of their kinetic energy, leading to mixed-valence superstructures [1]. Valence electrons are then almost localized on the atomic sites due to mutual repulsions. This condensation into an electron lattice, against a background of positive ion cores, is the so-called Wigner crystallization [2].

The prime example of CO studied for decades is the cubic spinel Fe$_3$O$_4$—magnetite or lodestone. Condensation of carriers to form an electron lattice, i.e. CO, occurs below the Verwey transition $T_V \sim 120$ K. At $T < T_V$, a superstructure of Fe$^{(3−\delta)+}$ and Fe$^{(2+\delta)+}$ mixed valence states occur ($\delta = 0$ for the case of fully ionic CO, increasing to $\delta = 0.5$ for no CO). The value of δ at $T < T_V$ is still a matter of controversy and may be of the order of 0.2–0.4 [3,4].

The iron oxoborate Fe$_2$OBO$_3$ invoked interest some years ago due to its close relation to magnetite [5,6]. If tetrahedral Fe^{3+} in Fe$_3$O$_4$ is selectively replaced by boron, the warwickite-structured Fe$_2$OBO$_3$ arises. Nearly integer iron valence separation into Fe^{2+} and Fe^{3+} occurs, as confirmed by Mössbauer effect spectroscopy, structural refinement, and electronic structure calculations [7–9], whereas the total charge disproportionation is small, of the order of 0.1 electron per site, in the majority of CO systems [1,10].

The LDA + U electronic-structure calculations for Fe$_2$OBO$_3$ showed that electron-electron correlations in the 3d shell of Fe play a significant role [8]. An insulating CO solution only appears when a strong on-site repulsion U of ~5.5 eV is included. The corresponding calculated energy gap in the electronic band structure amounts to ~0.4 eV, considered to be in reasonable agreement with the activation energies obtained from electrical transport experiments [5,11]. In the absence of U, a metallic solution exists without CO, at variance with experiments [5,7,11]. The difference of t_{2g}-orbital occupancies for Fe^{3+} and Fe^{2+} cations in Fe$_2$OBO$_3$ amounts to 80% of the ideal ionic CO model. This is considered the clearest case of (ionic) CO and is thus archetypal in that respect [7,8]. Moreover, this is primarily driven by the interplay of strong electron correlations manifested in the relatively large Hubbard U, in relation to the intersite Coulomb repulsion V.

Applied pressure modifies interatomic distances and accordingly tunes U/t and V/t electronic interaction parameters, where t is a pertinent transfer integral (hopping parameter determining 3d bandwidth) in an appropriately constructed Hamiltonian for the system. Quasi-low-dimensional structural features of Fe$_2$OBO$_3$ [5,12] and pressure tunability of short-range U/t and longer-range V/t are expected to stabilize interesting ground states [13]. This is also seen in quasi-low-dimensional organic systems investigated intensively in the last decade; for a review, see Ref. [14]. These involve regions of combinations of temperature T, U/t, and V/t phase planes, where CO insulator (COI, site ordered), CO fluctuations, dimer Mott insulator (DMI, bond-order type), metallization, and perhaps even superconductivity may occur [15–17].

Our recent magnetic-electronic study of Fe$_2$OBO$_3$ over an extended range up to ~30 GPa directly probed the Fe valence and demonstrated severe disruption to CO at ~16 GPa [18]. Electron exchange Fe^{2+} ⇔ Fe^{3+}, manifested as intermediate

---

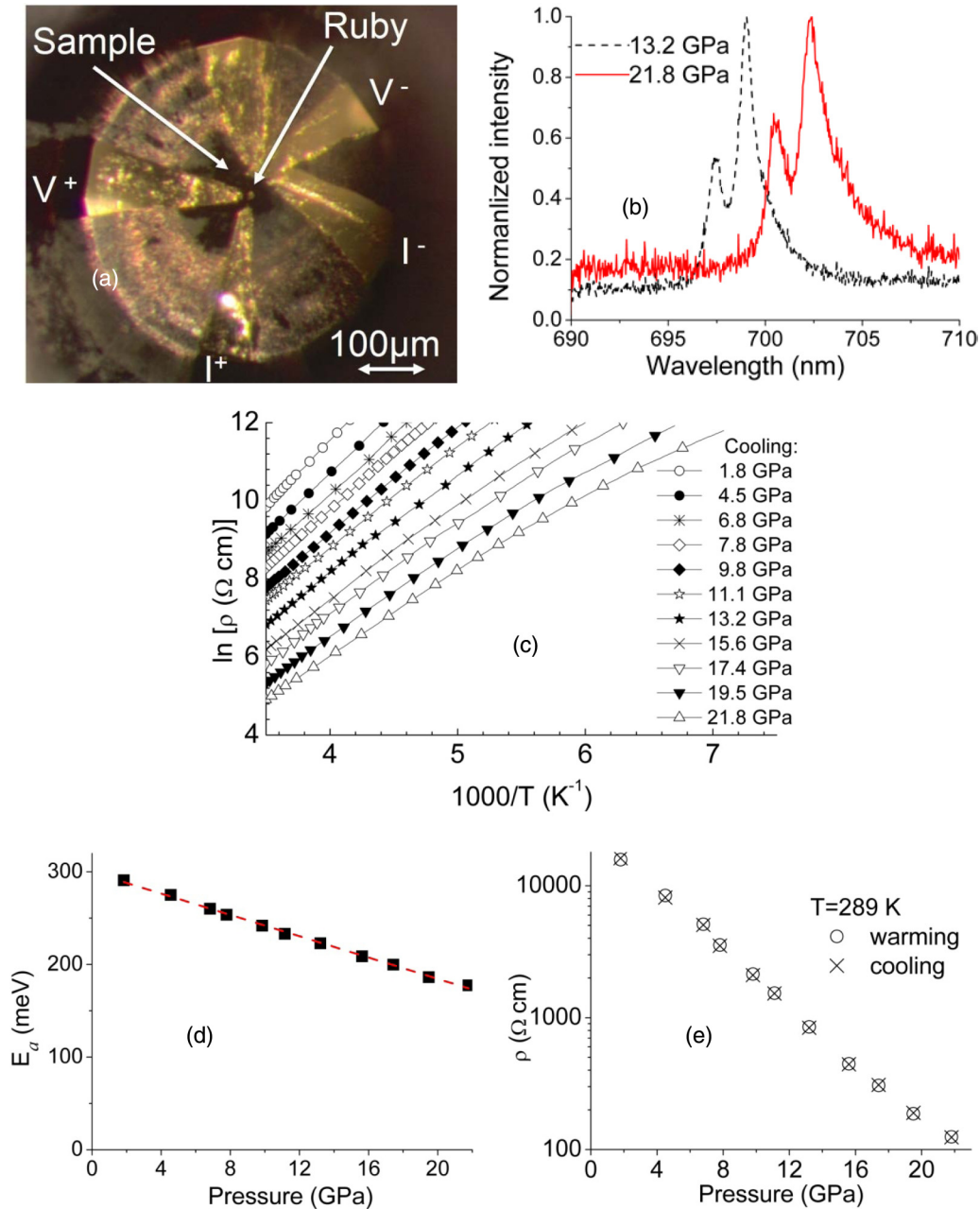*Corresponding author: grhearne@uj.ac.za

FIG. 1. (Color online) (a) Gold electrodes in a four-probe configuration within the pressurized sample cavity. (b) Examples of ruby fluorescence spectra at two different high pressures are plotted. This serves to illustrate that the fluorescence lines are well resolved to the highest pressure of this study, indicative of quasihydrostatic behavior. (c) Arrhenius plots, $\ln(\rho)$ versus $1000/T$ at different pressures. Solid lines are to guide the eye. (d) Activation energy E_a as a function of pressure extracted from the Arrhenius plots. (e) Plot of the resistivity at room temperature versus pressure.

valence signatures, is evidenced to well beyond this regime up to ~30 GPa. To gain better insight into the nature of the disruption of this Wigner-crystal type lattice, we have investigated the pressure response of both the electrical transport and x-ray diffraction (XRD) structural aspects to well beyond the CO instability (i.e. 16–30 GPa).

II. EXPERIMENTAL DETAILS AND RESULTS

Electrical-transport measurements at pressure have been performed using a diamond-anvil cell (DAC). Gold electrodes for four-probe measurements were channeled into the insulated microscopic sample cavity of the metallic gasket, see Fig. 1(a) [19]. Powdered sample from the same batch of the previous ^{57}Fe Mössbauer effect (ME) study was loaded into the insulated gasket hole [6,18]. A ruby ball for pressure determination was embedded in the sample powder, between the voltage leads [20].

Temperature-dependent resistance (R-T) data to ~22 GPa has been obtained by cycling to ~80 K in a home-developed electrical-transport station customized for the DAC, with a Si-diode in close proximity to determine temperature of the

sample. These are converted to estimates of resistivity (ρ-T) from sample and measurement geometry in Fig. 1(a). Cooling and heating curves were obtained at sufficiently low rates of 0.1–0.3 K minute^{-1} and showed no temperature hysteresis. Pressure was determined at room temperature from the change in wavelength $\Delta\lambda$ (nm) of the ruby R1 fluorescence line [21]. R1 and R2 fluorescence lines could still be well resolved to the highest pressures ($\sim$22 GPa) of the study, see Fig. 1(b), as an indicator of acceptable levels of hydrostaticity maintained in regions between the voltage leads.

The resistance-temperature behavior of Fe_2OBO_3 is that of a semiconductor (negative temperature coefficient) throughout the pressure range, 2–22 GPa, of this study. The semiconducting "gapped" behavior is best described by the following Arrhenius-type formulation for the resistivity, see Fig. 1(c):

$$\rho = \rho_0 e^{\frac{E_a}{k_B T}}, \tag{1}$$

where E_a is the activation energy.

Here, E_a values for each pressure, depicted in Fig. 1(d), were derived from Arrhenius plots involving Eq. (1) in the linear regime below 260 K. A value of $E_a = 300$ meV is extrapolated as the activation energy at ambient pressure, in good agreement with literature values [5,11]. The evolution of $E_a(P)$ shown in Fig. 1(d), yields a pressure dependence of $\sim$5.8 meV GPa^{-1}. Metallization is then estimated to occur at 50–60 GPa, assuming the activation energy would decrease continuously to zero following a linear trend. A similar inference can be drawn from the behavior of the resistivity estimate at room temperature versus pressure, Fig. 1(e). The sample resistivity is lowered by one decade per $\sim$8 GPa. Therefore, for the resistivity to reach 1 mΩ cm typical of metallic conduction in strongly correlated oxides ("bad metal") [22] would still require a drop of about 5 decades beyond 22 GPa. If there is no discontinuous electronic change in this high-pressure regime, typical metallic behavior ($d\rho/dT > 0$) would then occur at $\sim$60 GPa or beyond [23]. Evidently strong electron correlations ($U/t \gg 1$) and associated insulating behavior persist to extreme conditions, likely as high as 50–60 GPa. Prior ^{57}Fe ME studies have shown drastic disruption to the CO at $\sim$16 GPa [18], so electrical-transport measurements suggest that this CO instability is not associated with metallization.

The temperature pressure (T-P) regime at cryogenic temperatures below 16 GPa involves a Wigner electronic lattice (site centered Fe^{2+} minority-spin carrier localization, COI). At $\sim$16 GPa and well beyond this, our previous ^{57}Fe ME study demonstrated that $Fe^{2+} \Leftrightarrow Fe^{3+}$ electron exchange (on a time scale of $\sim$50 ns) prevails at all Fe sites. This is manifested in the spectral resonance profile and its centroid (isomer shift), which lies between the values typical for "ionic" Fe^{2+} and Fe^{3+} for $P > 16$ GPa [18]. Such hopping behavior, $Fe^{2+} \Leftrightarrow Fe^{3+}$, implies that the Fe^{2+} minority spin carriers are confined to Fe-Fe pairs (i.e. dimers) at high pressure. The accompanying insulating behavior that ensues, $P > 16$ GPa in Fig. 1, is different in nature to the site-centered localization at low pressure.

We have also investigated the structural response of the compound under pressure in XRD studies, to gain some insight into the nature of this insulating phase at high pressure [24]. Figure 2 shows selected XRD patterns of the structure at low
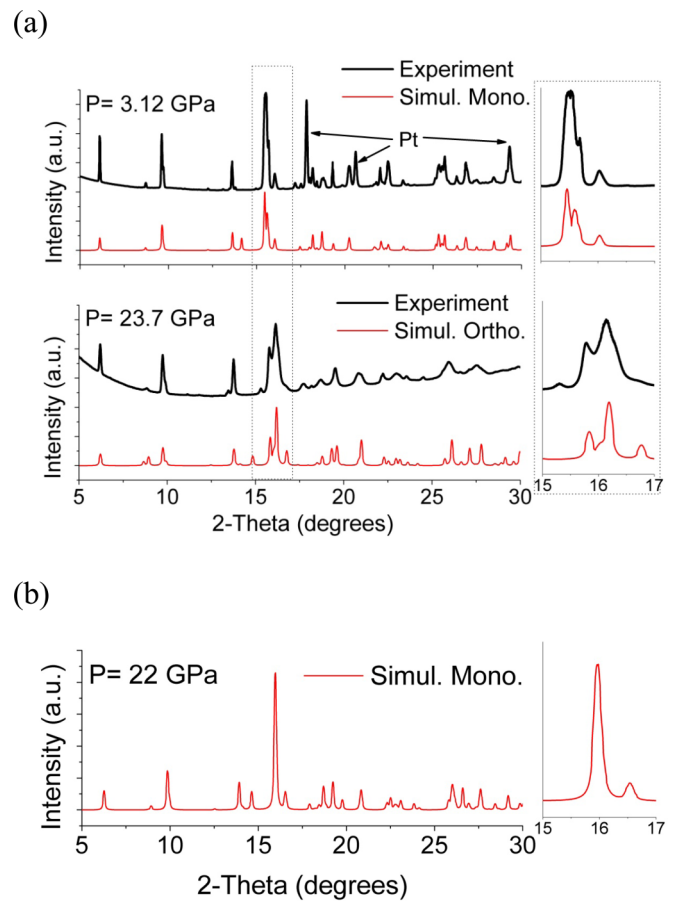

FIG. 2. (Color online) (a) Examples of x-ray diffraction patterns (black lines) taken from experiments at low and high pressures. These are accompanied by simulations (red lines) depicted below the experimental patterns to evidence the transition from a low-pressure monoclinic ($P2_1/c$) to a high-pressure orthorhombic ($Pmcn$) structural phase. Such simulations were obtained using lattice parameters derived from Rietveld refinements of the data (see text). Fingerprints of these phases are evident at the Bragg reflections near $\sim$16°, as shown in the expanded views in the right-hand columns. Reflections from the Pt pressure marker are shown in the spectrum at 3.12 GPa. (b) Simulation of the monoclinic phase pattern, were it to occur, as the dominant phase at high pressure, based on lattice parameters extrapolated from analysis of data at $P < 16$ GPa (see also Fig. 3). The reflections at $\sim$16° remain merged as a single intense feature irrespective of monoclinic angle used, unlike what is obtained in the experimental data at high pressure in (a).

pressure and at high pressure $P > 16$ GPa. This also has simulations of patterns for both the known (low-temperature COI) monoclinic phase ($P2_1/c$) and high-temperature orthorhombic phase ($Pmcn$) [7], using lattice parameters obtained from a Rietveld refinement of the XRD patterns at pressure [25]. These simulations as well as the nature of the splitting of the Bragg peaks at 16° (magnified in the right-hand panels of Fig. 2) are meant to exemplify that the high-pressure phase is also orthorhombic.

The Rietveld analysis of the XRD data indicates that a progressive monoclinic to orthorhombic phase conversion occurs spanning 6–22 GPa, see Fig. 3(a). The difference in unit cell volumes for the two coexisting phases in the structural
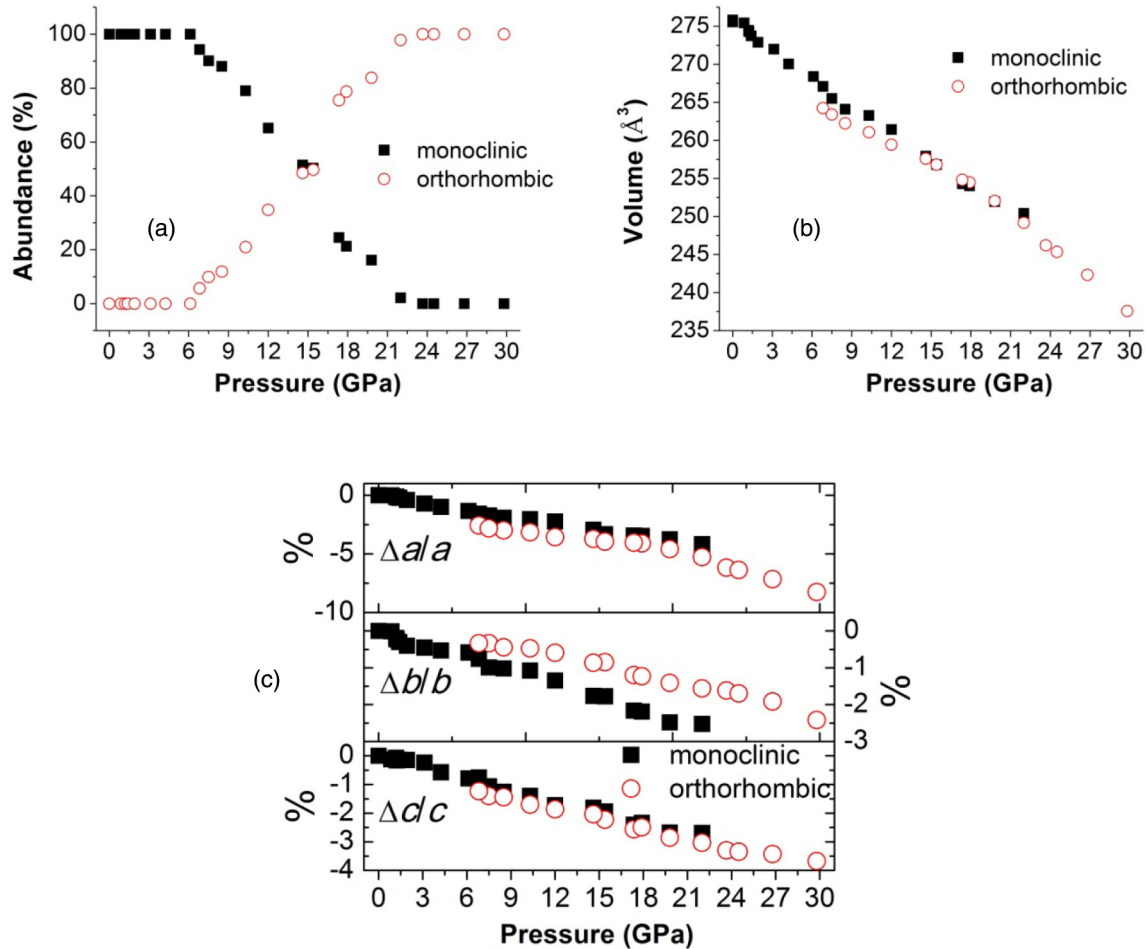
FIG. 3. (Color online) (a) Abundances of the monoclinic and orthorhombic structural phases as a function of pressure. The structural phases coexist in equal abundance at the CO destabilization pressure of $\sim$16 GPa where all Fe sites exhibit electron exchange, $Fe^{2+} \Leftrightarrow Fe^{3+}$. (b) Unit cell volume of the monoclinic phase and high-pressure orthorhombic phase as a function of pressure. (c) Relative change of the lattice parameters as a function of pressure, with respect to the values at ambient pressure having $a = 3.177$ Å as the shortest axis of the unit cell, $b = 9.387$ Å, and $c = 9.251$ Å.

evolution is small ($<$1%), Fig. 3(b). The resistivity data and gap values in Fig. 1 show no discontinuous change or change in pressure dependence at the CO destabilization at $\sim$16 GPa. This is likely because the structural transition does not involve a significant change in either unit cell volume or its pressure dependence as well, see Fig. 3(b), to within the accuracy of the fitted lattice parameters. Furthermore, the transition is somewhat sluggish and monoclinic and orthorhombic phases occur in equal abundances at $\sim$16 GPa in the structural conversion process that extends to beyond this electronic transition boundary. This may smear out any small change in resistivity or its pressure dependence if this occurs at the CO destabilization at $\sim$16 GPa. Resistivity-pressure measurements on single-crystals would be desirable to investigate this pressure regime in more detail, especially if changes in electrical-transport at the CO transition are anisotropic. However, having such samples to remain intact in the pressurized cavity to such extreme conditions would pose quite a severe experimental challenge, in addition to establishing ohmic contacts on such semiconducting microscopic fragments for pressurization in a hydrostatic pressure transmitting medium. Nevertheless, the pertinent outcome of our measurements, albeit on powdered

samples, is that the Fe_2OBO_3 system remains nonmetallic across the CO transition at $\sim$16 GPa.

The high-pressure state beyond $\sim$16 GPa is unlikely to be a new band insulator as a result of a drastic structural modification, based on the structural response depicted in Fig. 3(b), where the difference in unit cell volume of coexisting structural phases is less than 1%. The previous ^{57}Fe ME study [18] demonstrated that, beyond 16 GPa, distinct Fe valences are not discerned, and instead, a fluctuating or intermediate valence "$Fe^{2.5+}$" state occurs. This discounts a scenario of a strongly correlated phase involving site-centered charge localization in the high-pressure regime due to a strong on-site U, e.g. either a new mixed-valence COI state or single-valence Mott-Hubbard/charge-transfer antiferromagnetic insulator.

III. DISCUSSION

The combined observations that: (i) Fe_2OBO_3 is constituted by quasi-low-dimensional structural units, (ii) the high-pressure state involves electron hopping $Fe^{2+} \Leftrightarrow Fe^{3+}$ manifested as intermediate valence behavior, (iii) this state is nonmetallic as ascertained from the data in Fig. 1, and (iv)
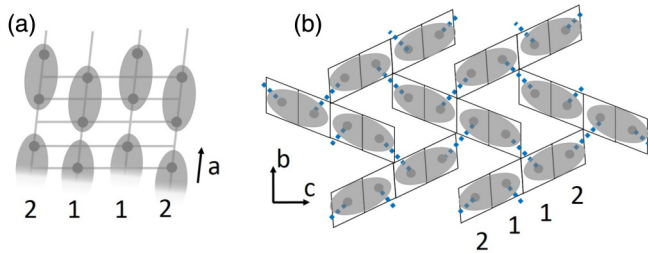
FIG. 4. (Color online) Schematic of quasi-low-dimensional aspects of the crystal structure (ribbons and chains). Crystallographic directions in the monoclinic unit cell have also been indicated. (a) Ribbon comprising four chains, extending infinitely along the *a* axis, with distinct Fe octahedral sites occurring in the outer chains Fe(2) and inner chains Fe(1). (b) The *b-c* plane showing stacked ribbons. Possibilities for $Fe^{2+} \Leftrightarrow Fe^{3+}$ electron exchange and associated charge carrier confinement to dimers (shaded ellipses) have been depicted. These would be enhanced in the orthorhombic phase (i.e. at high temperature or high pressure).
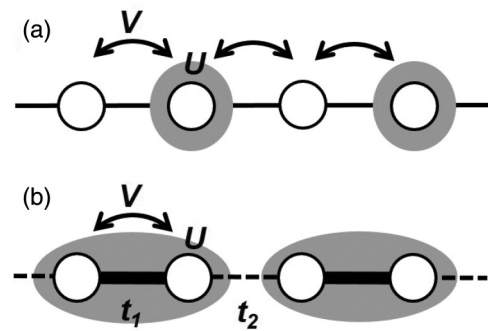

FIG. 5. Depiction of (a) CO insulator (Wigner electron lattice) and in (b) the DM insulator arising from dimerization, in a quasi-one-dimensional system as adapted from Ref. [14]. Shaded areas indicate regions of valence electron localization. Symbols V and U refer to intersite and on-site Coulomb repulsion, respectively. Thickness of the connecting line between sites signify magnitude of the charge transfer integral t.

the structural response is as depicted in Fig. 3, suggest that a somewhat unusual insulating high-pressure state occurs.

In the following, this high-pressure state is rationalized as possibly being a dimer Mott insulator involving bond-centered-type localization. This has close similarity to what has been predicted and observed in some quasi-low-dimensional systems; mainly organic conductors and in some cases transition-metal compounds [14].

At ambient pressure, Fe_2OBO_3 has a monoclinic unit cell in the COI state, comprising quasi-low-dimensional ribbons four chains wide running infinitely along the *a* axis, see Fig. 4. Ribbons stack laterally throughout the *b-c* plane [8,12]. The starting point for the theoretical description of such a COI in an array of low-dimensional (1D) lattice sites (chain) is given by the extended Hubbard model [14,17,26]:

$$H = -t \sum_i \sum_\sigma (c^\dagger_{i,\sigma} c_{i+1,\sigma} + \text{H.c.})$$
$$+ U \sum_i n_{i,\uparrow} n_{i,\downarrow} + V \sum_i n_i n_{i+1}, \qquad (2)$$

where t is the transfer integral between neighboring sites (related to pertinent 3*d* bandwidth*)*. Here, $c^\dagger_{i,\sigma}$ ($c_{i,\sigma}$) creates (eliminates) an electron of spin σ at the *i*th site along the chain, $n_{i,\sigma} = c^\dagger_{i,\sigma} c_{i,\sigma}$ and $n_i = n_{i,\uparrow} + n_{i,\downarrow}$. Besides the kinetic energy (first) term, it includes the on-site repulsion characterized by U and the nearest-neighbor Coulomb repulsion, parameterized by V. A strong on-site interaction U favors charge disproportionation (mixed-valence states). To account for long-range CO, intersite Coulomb repulsion V must be considered. In Fe_2OBO_3, U is of the order of 5–6 eV [8], $V \propto 1/r_{i,i+1}$ (intersite distance) is a fraction of 1 eV but may be up to 50% of U in some compounds, and t is typically a fraction of 1 eV [14]. The extended Hubbard Hamiltonian Eq. (2) applied to highly anisotropic cases of t (quasi-one-dimensionality) has been used to obtain the ground-state properties and construct phase diagrams for these systems, e.g. in the U-V plane. Charge order insulator behavior occurs at comparatively large U/t and V/t values at $T = 0$ K and CO fluctuations occur at finite T. As these Coulomb repulsion ratios decrease (e.g.

under pressure), a phase transition occurs to a metallic phase (Tomonaga-Luttinger liquid, TLL) in low dimensions (chains).

If interchain coupling is introduced into Eq. (2) [14,17]:

$$H^{<j,k>}_\perp = V_\perp \sum_i n_{i,j} n_{i,k} , \qquad (3)$$

where the summation is over pairs of adjacent sites on chains $\langle j,k \rangle$ and the strength of the interchain Coulomb repulsion is parameterized by $V_\perp$, then CO prevails at finite temperatures in the T-(V/t) phase diagram with appropriately large values of U/t and V/t [27]. Metallization is still anticipated to occur below a critical value of V/t, as exemplified in various quasi-low-dimensional molecular conductors [14,28]. Applied pressure affects inter- and intrachain distances, thus tuning U/t and V/t to the extent that metallic behavior ensues when CO is destabilized. This has been exemplified in organic compounds where the pressure evolution from COI to metallic behavior occurs, e.g. in DI-$DCNQI_2Ag$ [28].

In Fe_2OBO_3 at ~16 GPa, metallization does not ensue, although CO is destabilized—see one of the main results of this investigation, in Fig. 1. A different insulating phase prevails to well beyond ~16 GPa, in which site-centered CO is absent. Such insulator-to-insulator transitions have also been investigated in quasi-low-dimensional systems which evolve from an original COI state [27,29]. Charge localization may persist and change from being site centered to bond-centered type if a strongly anisotropic t prevails, involving modulated hopping strengths t_1 and t_2 amongst site pairs along the chain direction where it is strongest, see Fig. 5. This "dimerization", depicted in Fig. 5(b), may be intrinsic as originated from bonding/structural anisotropy typical of quasi-low-dimensional systems. Alternatively, such dimerization may be spontaneous arising from electron-lattice coupling in Peirels-type distortions, provided that the elastic energy cost does not supersede the electronic energy gain. Both such intrinsic and spontaneous dimerization are incorporated in the kinetic term of the quasi-one-dimensional extended Hubbard

Hamiltonian as follows [17]:

$$H = \sum_j H_{1D}^j + \sum_{\langle jk \rangle} H_\perp^{\langle jk \rangle}, \tag{4a}$$

where

$$
\begin{aligned}
H_{1D}^j &= -\sum_i \sum_\sigma ([t+(-1)^i \delta_D](1+u_{i,j})[c_{i,j,\sigma}^\dagger c_{i+1,j,\sigma} + \text{H.c.}]) \\
&\quad + \frac{K_p}{2}\sum_i u_{i,j}^2 + U\sum_i n_{i,j,\uparrow} n_{i,j,\downarrow} + V\sum_i n_{i,j} n_{i+1,j}.
\end{aligned}
\tag{4b}
$$

The modulation of t, as $t - \delta_D$ and $t + \delta_D$, arises from low dimensionality features and structural details or is originated from a lattice distortion $u_{i,j}$ (at site i in the jth chain). Here, K_p is the elastic coupling constant, and there may be higher-order terms. The terms in Eq. (4b) represent the intrachain part. The term $H_\perp^{\langle jk \rangle}$ is the interchain part [Eq. (2)] leading to CO transitions at finite temperature. Sufficiently strong dimerization leads to the dimer Mott insulator (DMI) ground state instead of metallization, in appropriate regions of the U/t-V/t phase plane [17,29]. In contrast to charge being localized on every alternate site (COI), rather, valence charge localizes on every pair of sites (dimers), schematized in Fig. 5. The "on-dimer" U now plays the crucial role of inhibiting dimer to dimer hopping (DMI). The system evolves from the COI ground state at large U/t and V/t values to the DMI state upon tuning these ratios to smaller values (e.g. by pressure to increase bandwidth t). That is, an insulator-to-insulator transition involving persistent electron correlations may occur [27,29].

The ribbon and chain features of the warwickite structure and how it sustains CO are depicted in Fig. 4. Charge order is predicted to thread along the chains of the a axis, Fig. 4(a) [8]. Electronic structure calculations reveal the most favorable charge transfer paths conducive to hopping and thus dimer formation [8,30]. They may be paths involving crystallographically similar sites [e.g. Fe(1)O$_6$-Fe(1)O$_6$] within chains comprising a ribbon, Fig. 4(a). Intrinsic modulation of t along the a axis within a chain is absent. Therefore, dimer formation along the quasi-one-dimensional chains would need to be spontaneous Peierls type involving a lattice distortion, when energetically favored in the structure by a high enough compressibility in that direction [7,31]. Alternatively, Fig. 4(b) shows inter-intra-inter-intra-... ribbon sequences in the c axis direction which involve an intrinsic modulation of t, similar to Fig. 5(b). Both scenarios of Fig. 4 would be similarly represented in the orthorhombic phase (e.g. at high temperature at ambient pressure) where the hopping integrals are appreciably enhanced [30].

The structural response of Fe$_2$OBO$_3$ at pressure, depicted in Fig. 3, favors the dimerization portrayed in Fig. 4. The orthorhombic structure at high pressure has a local geometry more favorable to intraribbon hopping of Fig. 4 as indicated in semi-empirical electronic structure calculations [30]. Figure 3(c) shows the relative change in lattice parameters at pressure. The changes in a and c axes are compatible with the dimerization schemes of Fig. 4. The shorter a axis of the unit cell is much more compressible than other

crystallographic directions. Spontaneous Peierls-type dimerization would therefore be favored to occur along this direction.

Previous ^{57}Fe ME data show an average valence of Fe$^{2.5+}$ at all Fe sites as a result of the electron exchange [18]. This supports the notion of dimer formation in the electron-exchange process Fe^{2+} $\Leftrightarrow$ Fe^{3+}, and not larger units like trimers that occur in Fe$_3$O$_4$ [4]. These are prevalent in both structural phases which have equal abundances at 16 GPa, see Fig. 3(a).

Pressures to 30 GPa primarily tune the modulated t, described in Eq. (4), such that Fe$_2$OBO$_3$ evolves from COI in the U/t-V/t phase plane to where the DMI phase is stabilized [27,29]. This may be compared with Fe$_3$O$_4$ in the same pressure regime, where an insulator-metal transition ensues [32]. The contrasting pressure responses of Fe$_3$O$_4$ and Fe$_2$OBO$_3$ may partly be ascribed to the difference in starting (ambient) pressure ground states. The COI state in Fe$_3$O$_4$ involves electron localization over three-Fe-site units (a first-approximation Fe^{2+} site and two Fe^{3+} neighbors) [4]. This creates "trimeron" distortions with short Fe-Fe distances and reduces the charge separation in the Fe$^{(3-\delta)+}$ and Fe$^{(2+\delta)+}$ superstructure to $\delta \sim 0.4$ [3,4], compared with ionic CO ($\delta \sim 0$) in Fe$_2$OBO$_3$ [7].

IV. CONCLUSION

The pressure-induced CO instability at ~16 GPa in Fe$_2$OBO$_3$ can be rationalized as a change from site-centered to dimer-centered (bond centered type) charge localization, COI $\to$ DMI transition. Persistent insulating behavior at $P >$ 16 GPa in tandem with evidence of Fe^{2+} $\Leftrightarrow$ Fe^{3+} electron exchange and associated "Fe$^{2.5+}$" intermediate valence at all sites, from a previous direct probe of the Fe electronic state using ^{57}Fe ME spectroscopy, supports the notion of electron confinement to Fe-Fe dimers and not new site-centered localization. The structural response of the system gleaned from XRD pressure studies evidences a sluggish monoclinic-to-orthorhombic transition without a significant change in unit cell volume associated with the structural adjustment. These observations suggest that the insulating high-pressure phase is unlikely to be a new band insulator that would emanate from a significant change in structure, nor is it either a new COI state or antiferromagnetic Mott insulator, both of which involve site-centered localization. Rather, there are the prerequisite quasi-low-dimensional features in the structure (chains and ribbons) and attendant anisotropy and modulation in the relevant transfer integrals t, for stabilizing a DMI ground state when both pertinent Coulomb repulsion parameters U/t and V/t are varied under pressure. Modulation in t arises either spontaneously in Peierls-type distortions along the much more compressible a axis or else originates from intrinsic features in the c axis direction. This is compatible with the structural pressure response which evidences both a monoclinic $\to$ orthorhombic transition that enhances these transfer integrals as well as a unit cell deformation response, involving a comparatively pronounced a axis compressibility, that supports the proposed dimerization schemes. Furthermore, reduced intra- and interribbon spacings under applied pressure enhance interactions between the ribbons and chains V$_\perp$, which also favor transitions between such COI/DMI ground states.

[1] J. P. Attfield, Solid State Sciences **8**, 861 (2006).

[2] E. Wigner, Phys. Rev. **46**, 1002 (1934).

[3] J. P. Wright, J. P. Attfield, and P. G. Radaelli, Phys. Rev. Lett. **87**, 266401 (2001).

[4] M. S. Senn, J. P. Wright, and J. P. Attfield, Nature **481**, 173 (2011).

[5] J. P. Attfield, A. M. T. Bell, L. M. Rodriguez-Martinez, J. M. Greneche, R. J. Cernik, J. F. Clarke, and D. A. Perkins, Nature **396**, 655 (1998).

[6] J. P. Attfield, A. M. T. Bell, L. M. Rodriguez-Martinez, J. M. Greneche, R. Retoux, M. Leblanc, R. J. Cernik, J. F. Clarke, and D. A. Perkins, J. Mater. Chem. **9**, 205 (1999).

[7] M. Angst, P. Khalifah, R. P. Hermann, H. J. Xiang, M.-H. Whangbo, V. Varadarajan, J. W. Brill, B. C. Sales, and D. Mandrus, Phys. Rev. Lett. **99**, 086403 (2007).

[8] I. Leonov, A. N. Yaresko, V. N. Antonov, J. P. Attfield, and V. I. Anisimov, Phys. Rev. B **72**, 014407 (2005).

[9] At low temperatures $T < 280$ K, the electronic system is commensurately charge ordered, with its basic charge-ordered units being chains of alternating valences, Fe^{2+} and Fe^{3+}, running along the a axis of the monoclinic unit cell. The total charge order is established over domains. These are large in the a and b directions, but of small size along the c axis. In a slightly higher temperature range, for 280 K $< T < 340$ K, the incommensurate phase occurs. It arises due to easy domain wall creation, which results most likely from a compromise between the tendency to charge ordering and the geometrical frustration for interactions between chains and ribbons of the quasi-low-dimensional structure. At $T > 340$ K, CO is disrupted.

[10] Yundi Quan, V. Pardo, and W. E. Pickett, Phys. Rev. Lett. **109**, 216401 (2012).

[11] A. P. Douvalis, V. Papaefthymiou, A. Moukarika, T. Bakas, and G. Kallias, J. Phys.: Condens. Matter **12**, 177 (2000).

[12] M. Angst, R. P. Hermann, W. Schweika, J.-W. Kim, P. Khalifah, H. J. Xiang, M.-H. Whangbo, D.-H. Kim, B. C. Sales, and D. Mandrus, Phys. Rev. Lett. **99**, 256402 (2007).

[13] A. Akrap, M. Angst, P. Khalifah, D. Mandrus, B. C. Sales, and L. Forró, Phys. Rev. B **82**, 165106 (2010).

[14] H. Seo, C. Hotta, and H. Fukuyama, Chem. Rev. **104**, 5005 (2004).

[15] K. C. Ung, S. Mazumdar, and D. Toussaint, Phys. Rev. Lett. **73**, 2603 (1994).

[16] H. Yoshioka, M. Tsuchiizu, and H. Seo, J. Phys. Soc. Jpn. **75**, 063706 (2006).

[17] H. Yoshioka, Y. Otsuka, and H. Seo, Crystals **2**, 996 (2012).

[18] G. R. Hearne, W. N. Sibanda, E. Carleschi, V. Pischedda, and J. P. Attfield, Phys. Rev. B **86**, 195134 (2012).

[19] A Merill-Basset (opposing plates) DAC comprised of Inconel low thermal expansion components has been used for the variable-temperature electrical-transport measurements to elevated pressures. The metallic gasket has been insulated with a mixture of Stycast 1266 and Al_2O_3 powder of 0.3-μm grain size. The sample has been confined in a $\phi \sim 100$-μm insulating ring within the insulated metallic gasket cavity. Flattened gold wires were used for the electrodes in the experiment in standard four-probe measurements. An excitation current of 1 μA has been used, and the measured voltage was between two leads spaced ~ 50 μm apart. The leads were configured so as to be able to establish that there is continuity of the electrodes leading into the cavity (useful in the case of insulating/semiconducting samples).

[20] This permits measurement of pressure in the vicinity of where the voltage difference is detected. It also enables a check for the degree of hydrostaticity, through the resolution of the ruby R1 and R2 fluorescence peaks. No pressure-transmitting medium has been used, and the pressure is presumably transmitted through the relatively soft sample and surrounding soft insulating materials.

[21] N. Tateiwa and Y. Haga, Rev. Sci. Instrum. **80**, 123901 (2009).

[22] N. E. Hussey, K. Takenaka, and H. Takagi, Phil. Mag. **84**, 2847 (2004).

[23] Electrical transport measurements at higher pressure beyond ~ 22 GPa were not attempted because of the perceived risk of anvil failure, given the rather large diamond culet sizes used here (~ 550 μm). Moreover, from these extrapolations, it is clear that appreciably higher pressures $P > 30$ GPa would be needed to render the sample metallic. It may be noted that the highest pressure attained here ~ 22 GPa is sufficiently well beyond where the previous ^{57}Fe ME data reveals a disruption of CO at ~ 16 GPa.

[24] Angle dispersive XRD measurements were performed at the ELETTRA synchrotron (Trieste-Italy). Miniature piston-cylinder DACs were used to attain high pressures for the studies at a wavelength of 0.70001 Å. Daphne oil was used as a pressure transmitting medium. Two separate compression runs to high pressure, 24–30 GPa, were completed at 300 K. Pressure estimates were obtained from the equation-of-state (EOS) of a piece of platinum loaded in the cavity (150–250 μm diameter) containing the sample. We could locate the beam (~ 70 μm diameter) in the center of the pressurized cavity to measure predominant platinum reflections and thus estimate pressure, or have the beam slightly off the center (by 30–50 μm) of the piece of platinum to obtain the diffraction pattern dominated by sample reflections. Numerous patterns were taken in pressure increments of 2–3 GPa. Results of the detailed analysis of the data will be published elsewhere.

[25] V. Petricek, M. Dusek and L. Palatinus, (2006). Jana2006. The crystallographic computing system. Institute of Physics, Praha, Czech Republic.

[26] H. Seo and H. Fukuyama, Synthetic Metals **133–134** 257 (2003).

[27] H. Yoshioka, M. Tsuchiizu, and H. Seo, J. Phys. Soc. Jpn. **76**, 103701 (2007).

[28] T. Itou, K. Kanoda, K. Murata, T. Matsumoto, K. Hiraki, and T. Takahashi, Phys. Rev. Lett. **93**, 216408 (2004).

[29] M. Tsuchiizu, H. Yoshioka, and Y. Suzumura, J. Phys. Soc. Jpn **70**, 460 (2001).

[30] M. Matos and R. B. Oliveira, J. Phys.: Condens. Matter **18**, 8267 (2006).

[31] A lattice distortion associated with the dimerization changes the lattice periodicity. Intersite transfer integrals would be modulated in the process. Energy gaps appear at the new Brillouin zone boundaries, and energies of occupied electronic states decrease, resulting in electronic energy gain. Such a lattice distortion u_i is favored if the electronic energy gain, $\sim(\ln u_i)u_i^2$, exceeds the elastic energy cost to deform the lattice $\sim \frac{1}{2}K_p u_i^2$, where K_p is related to the compressibility. See D. Khomskii, *Basic aspects of the quantum theory of solids: order and elementary excitations* (Cambridge Univ. Press, Cambridge England, 2010).

[32] N. Môri, S. Todo, N. Takeshita, T. Mori, and Y. Akishige, Physica B **312–313**, 686 (2002).